Effect of Layer Stacking on the Electronic Structure of Graphene Nanoribbons

Neerav Kharche,[†,‡,*] Yu Zhou,[‡] Kevin P. O'Brien,[§] Swastik Kar,[⊥] and Saroj K. Nayak[‡,*]

[†]Computational Center for Nanotechnology Innovations, [‡]Department of Physics, Applied Physics and Astronomy, Rensselaer Polytechnic Institute, Troy, New York 12180, United States, [§]Intel Corporation Components Research, Hillsboro, Oregon 97124, United States, and [⊥]Department of Physics, Northeastern University, Boston, Massachusetts 02115, United States

ABSTRACT The evolution of electronic structure of graphene nanoribbons (GNRs) as a function of the number of layers stacked together is investigated using *ab initio* density functional theory (DFT), including interlayer van der Waals interactions. Multilayer armchair GNRs (AGNRs), similar to single-layer AGNRs, exhibit three classes of band gaps depending on their width. In zigzag GNRs (ZGNRs), the geometry relaxation resulting from interlayer interactions plays a crucial role in determining the magnetic polarization and the band structure. The antiferromagnetic (AF) interlayer coupling is more stable compared to the ferromagnetic (FM) interlayer coupling. ZGNRs with the AF in-layer and AF interlayer coupling have a finite band gap, while ZGNRs with the FM in-layer and AF interlayer coupling do not have a band gap. The ground state of the bilayer ZGNR is nonmagnetic with a small but finite band gap. The magnetic ordering is less stable in multilayer ZGNRs compared to that in single-layer ZGNRs. The quasiparticle GW corrections are smaller for bilayer GNRs compared to single-layer GNRs because of the reduced Coulomb effects in bilayer GNRs compared to single-layer GNRs.

KEYWORDS: graphene nanoribbons · electronic structure · GNR magnetism · graphene interconnects · quasiparticle band gaps

Graphene has attracted enormous attention due to its extraordinary electronic, optical, thermal, and mechanical properties and immense potentials for nanoelectronic applications.[1−7] This single-atom thick, sp^2-hybridized allotrope of carbon with a perfectly 2D confinement of its electronic states is a zero-gap semimetal, exhibiting a linear dispersion relation $E(\mathbf{k}) = \hbar v_F k$ near the meeting point of its conical valence and conduction bands (the Dirac point).[3] Graphene can conduct much higher current densities than currently used Cu interconnects in the integrated circuits (ICs).[8,9] Graphene also exhibits much higher carrier mobilities compared to the conventional field-effect transistor (FET) channel materials such as Si and III−V groups.[2] These unique electronic properties make graphene one of the most promising candidate materials for both transistors and interconnects in future ICs.[10]

For many practical applications, such as in nanoelectronic devices, graphene needs to be patterened into the so-called graphene nanoribbons (GNRs). Typically, graphene is patterned by selectively removing the material by physical etching techniques. Graphene can also be patterned by selective chemical functionalization with hydrogen[11,12] or fluorine,[13,14] which results in graphene nanostructures embedded in functionalized graphene: typically a wide band gap insulator. The electronic properties of GNRs are very sensitive to their width and edge geometry.[15−18] The dependence of edge geometry on the electronic structure of GNRs has been mainly investigated using theoretical approaches, such as the tight-binding model and density functional theory (DFT). Theoretical studies indicate that the band gap of single-layer armchair GNRs (AGNRs) is extremely sensitive to their width.[16,17] Antiferromagnetic ordering at the edges of zigzag GNRs (ZGNRs) opens up a band gap, while ferromagnetically ordered ZGNRs do not have a band gap.[16,17] The band gap in both AGNRs and ZGNRs can be controlled by an external electric field.[18] Experimental observations of these theoretical predictions remain elusive due to the challenging task of atomically precise control of the GNR edges. The available state-of-the-art transport measurements[15,19] are performed on GNRs with a width on the order of 10 nm; however, their edges are rough, making direct quantitative comparison with theory difficult. The experimental techniques, however, keep improving at a rapid pace. For example, the magnetic ordering at the edges predicted by DFT calculations[16,17] has been recently observed in GNRs with ultrasmooth edges.[20]

Layer stacking provides an additional handle to tune the electronic properties of graphene and GNRs through interlayer interactions. The effect of layer stacking in graphene has been extensively studied

* Address correspondence to kharcn@rpi.edu, nayaks@rpi.edu.

Received for review March 11, 2011 and accepted July 18, 2011.

10.1021/nn200941u

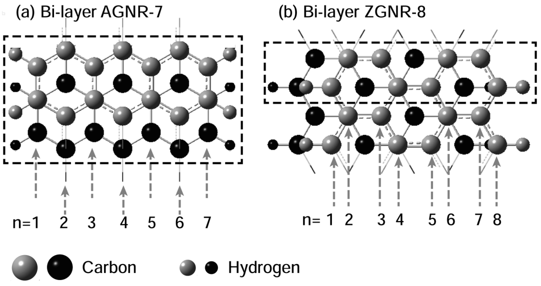

Figure 1. Schematics of simulated structures. AB Bernal stacking in (a) AGNR-7 and (b) ZGNR-8. Gray and black colored atoms belong to top and bottom layers, respectively. The unit cells are depicted by the dashed rectangles.

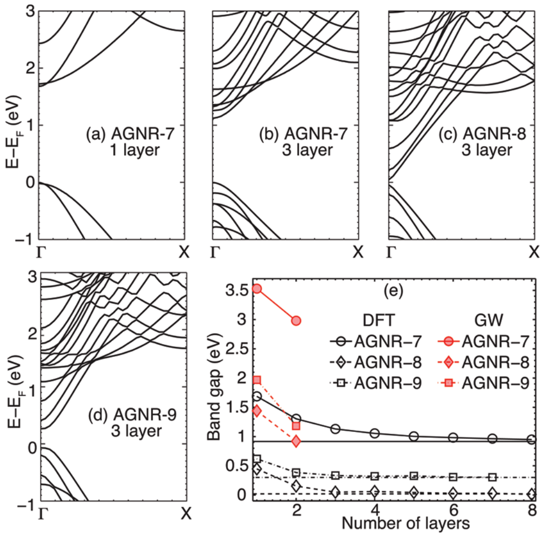

Figure 2. Band structure of single- and trilayer AGNRs belonging to three classes 3*p*, 3*p* + 1, and 3*p* + 2 depending on their width. (a) Single-layer AGNR-7, (b) trilayer AGNR-7, (c) trilayer AGNR-8, and (d) trilayer AGNR-9. (e) DFT band gaps (open symbols) of AGNRs as a function of the number of layers. The horizontal lines show the DFT band gaps of multilayer AGNRs obtained by applying periodic boundary conditions in the thickness direction. The solid symbols are the GW-corrected band gaps of single- and bilayer AGNRs.

theoretically.[21−25] Recent experiments have demonstrated tuning of electronic properties of graphene by layer stacking. For example, (i) a band gap can be opened up in a bilayer graphene by applying an electric field;[26] (ii) trilayer graphene behaves like a semimetal in the presence of an electric field;[27] and (iii) multilayer graphene shows a peculiar conductivity spectra depending on the number of layers.[28,29] There have been several theoretical studies on the electronic structure of bilayer GNRs;[30−34] however, similar studies beyond bilayer stacking are lacking except in ref 35, where the effects of geometry relaxation were not included.

In this paper, we report an investigation of the effect of layer stacking on the electronic structure of armchair and zigzag GNRs using *ab initio* density functional theory (DFT). Interlayer van der Waals interactions are included to accurately model the effects of geometry relaxation on the electronic structure. The width and thickness dependence of the electronic structure of multilayer AGNRs is discussed first, then the energetics of geometry relaxation and magnetic ordering and their effects on the electronic structure of multilayer ZGNRs are discussed.

It should be pointed out here that DFT-based calculations underestimate the band gap of GNRs, and perturbative correction schemes such as the GW method should be used to obtain accurate estimates.[17] GW calculations are computationally much more expensive compared to DFT. Since the primary goal here is to study the evolution of electronic structure as a function of the number of layers rather than quantitatively estimate the band gaps of stacked GNRs, we have used the computationally less expensive DFT scheme for most of the calculations. The more accurate GW-corrected band gaps are calculated for single-layer and bilayer GNRs to provide an estimate of the quasiparticle corrections in these nanostructures.

The atomistic schematics of simulated bilayer AGNRs and ZGNRs with AB Bernal stacking are shown in panels a and b of Figure 1, respectively. For three and more layers, ABA and ABAB... stackings are used. An interlayer distance of 3.35 Å (same as graphite) is used as a starting point in the geometry optimization. Edges of GNRs are passivated with hydrogen. Henceforth, 1−8 layer thick GNRs are referred to as few-layer GNRs, while multilayer GNR refers to a GNR obtained by applying periodic boundary conditions to a bilayer GNR in the thickness direction.

RESULTS AND DISCUSSION

The electronic structure of AGNRs is discussed first. The band structure of a single-layer and a trilayer AGNR-7 is shown in Figure 2a,b, respectively. As the three AGNR-7 layers are moved closer to form a trilayer AGNR-7, the three-fold band degeneracy is lifted due to the interlayer coupling and the band gap is reduced. Thus, the degenerate bands in each of the three single-layer AGNR-7 results in three nondegenerate bands in a trilayer AGNR-7. All few-layer AGNRs show a similar band structure evolution. As shown in Figure 2e, the band gap of AGNR-7 gradually decreases as the number of layers increases and shows a tendency to approach the multilayer AGNR-7 limit. The comparison of the band structures of trilayer AGNR-7 (Figure 2b), AGNR-8 (Figure 2c), and AGNR-9 (Figure 2d) illustrates the fact that similar to single-layer AGNRs trilayer AGNRs show three classes (*i.e.*, $N = 3p$, $3p + 1$, and $3p + 2$, where N denotes the number of carbon chains along the width and p is an integer) of band structures depending on their width. Similar to AGNR-7, AGNR-8 and AGNR-9 show convergence of the band gap to the multilayer limit (Figure 2e). This classification was recently reported in ref 35 for up to four-layer thick AGNRs. Figure 2e indicates that this classification persists beyond four layers.

The GW-corrected band gaps of single- and bilayer AGNRs are also shown in Figure 2e. Large quasiparticle corrections on the order of 1−2 eV are attributed to enhanced Coulomb effects.[17] Compared to bulk, GNRs are under confinement and have greatly reduced screening, which enhances the Coulomb effects. The quasiparticle corrections for bilayer AGNRs are smaller compared to those for single-layer AGNRs. This is because each layer screens the Coulomb interactions in another layer, reducing the overall Coulomb effects.[36−40]

ZGNRs show an edge magnetism, which can have multiple configurations depending on relative in-layer and interlayer spin polarizations.[15−18,31−35] The two possible spin polarizations in a single-layer ZGNR are (i) ferromagnetic (FM) in-layer and (ii) antiferromagnetic (AF) in-layer, while multilayer ZGNRs can have several possible spin polarizations. The four spin polarizations in multilayer ZGNRs investigated here are (i) FM−FM, FM in-layer and FM interlayer; (ii) AF−FM, AF in-layer and FM interlayer; (iii) FM−AF, FM in-layer and AF interlayer; and (iv) AF−AF, AF in-layer and AF interlayer. Multilayer ZGNRs initialized in configurations (iii) and (iv) stay in those configurations, while multilayer ZGNRs initialized in configurations (i) and (ii) converge to configuration (iv), which indicates that the FM interlayer coupling is not as stable as the AF interlayer coupling. Reference 32 also reported that the AF interlayer coupling has lower energy compared to the FM interlayer coupling. Therefore, AF interlayer coupling is used in all ZGNR electronic structure calculations presented in this article.

The relaxation energy (*i.e.*, difference between total energy of relaxed and unrelaxed) ZGNRs as a function of the number of layers is plotted in Figure 3a. Both nonmagnetic (NM) and magnetically ordered ZGNRs show similar trends in the relaxation energy as a function of the number of layers. Due to the interlayer van der Waals attraction, the top and bottom layers show a concave curvature while the other layers remain more or less flat. Similar curvatures were reported in ref 31 for the bilayer ZGNR. This concave curvature is the main cause of the reduction in total energy of the relaxed few-layer ZGNRs. The relaxation energy of the single-layer ZGNR is negligible because of the absence of curvature.

Figure 3b shows the magnetic stabilization energy ($\Delta E_M = E_{NM} - E_M$) of unrelaxed ZGNRs resulting only from the FM−AF and AF−AF orderings at the edges. ZGNRs with AF−AF and FM−AF orderings both show similar trends as a function of the number of layers, such that ZGNRs with AF in-layer configuration are lower in energy compared to ZGNRs with FM in-layer coupling. ΔE_M is much smaller in ZGNRs with two or more layers compared to the single-layer ZGNR. This implies that the interlayer interactions weaken the strength of magnetic ordering in each layer of the few-layer ZGNRs.[41] The interlayer interactions become stronger in relaxed ZGNRs because of the concave curvature in the top and bottom layers. This further weakens the strength of in-layer magnetic coupling, which results in lower energy difference between magnetic and nonmagnetic states of relaxed ZGNRs compared to unrelaxed ZGNRs (Figure 3b,c).

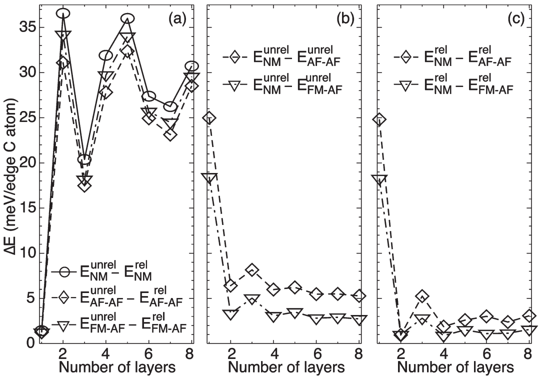

Figure 3. Energetics of ZGNR-8. Difference between total energy of (a) relaxed and unrelaxed ZGNRs, (b) magnetically ordered and nonmagnetic unrelaxed ZGNRs, and (c) magnetically ordered and nonmagnetic relaxed ZGNRs as a function of the number of layers.

The bilayer ZGNRs initialized in both the FM−AF and AF−AF configurations converge to a nonmagnetic ground state when the geometry relaxation is allowed. Therefore, in the bilayer ZGNR, there is no reduction in the total energy due to the magnetic ordering (Figure 3c). Reference 31, which included van der Waals interactions, also reported that the ground state of bilayer ZGNRs is nonmagnetic. In the calculations, where the geometry relaxation is not included, the bilayer ZGNRs initialized in the FM−AF and AF−AF configurations stay in those configurations and do not converge to a nonmagnetic ground state (Figure 3b).

The calculated ΔE_M of relaxed ZGNRs (Figure 3c) is comparable to the thermal energy at room temperature ($k_BT \approx 25$ meV), which indicates that magnetic ordering is unstable at room temperature. The layer stacking destabilizes edge magnetism by reducing ΔE_M. The roughness and reconstruction at the ZGNR edges further destabilize the magnetic ordering even at low temperatures. Thus, the magnetic ordering is expected to manifest at low temperatures in single-layer ZGNRs with atomically smooth edges. Indeed, the edge magnetism was observed recently at low temperatures in GNRs with atomically smooth edges slightly offset from an ideal zigzag edge.[20]

The band structures of 1−4 layer thick relaxed ZGNRs in the nonmagnetic, AF−AF, and FM−AF configurations are shown in Figure 4. Nonmagnetic ZGNRs have nearly flat bands near the Fermi level (E_F) leading to high density of states (DOS) near E_F. The bands near E_F are mainly composed of the edge states. The high DOS near E_F gives rise to magnetic instability, and the edge states become spin-polarized.[16] The up and

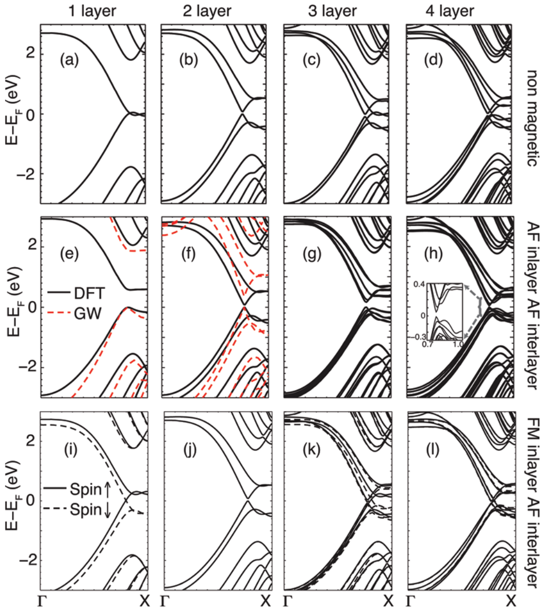

Figure 4. DFT band structures of 1−4 layer ZGNR-8 in nonmagnetic (a−d), antiferromagnetic (AF) in-layer and AF interlayer (e−h), and ferromagnetic (FM) in-layer and AF interlayer (i−l) configurations. Single-layer ZGNRs do not have AF interlayer couplings. Inset in (h) shows a zoomed-in view of the band structure near the band gap. The dotted lines in (e) and (f) are the GW-corrected band structures. The up and down spin states in (e−h) are degenerate, while they are nondegenerate in (i−l).

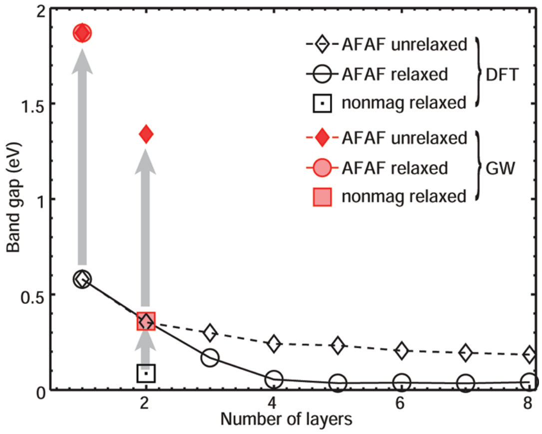

Figure 5. DFT band gaps (open symbols) of relaxed and unrelaxed ZGNRs in AF−AF configuration as a function of the number of layers. The band gap of relaxed bilayer ZGNR, which has a nonmagnetic ground state, is depicted by an open square. The corresponding GW-corrected band gaps of single- and bilayer ZGNRs are depicted by the solid symbols.

down spin states in ZGNRs with AF−AF ordering at the edges are degenerate, while they are split in ZGNRs with FM−AF ordering. The AF in-layer coupling at the edges opens up a band gap, while FM in-layer coupling does not. The band structures of 5−8 layer thick relaxed ZGNRs are not shown here but are qualitatively similar. The band structures of the bilayer ZGNR in the AF−AF (Figure 4f) and FM−AF (Figure 4j) configurations are identical to nonmagnetic band structure (Figure 4b) because the bilayer ZGNRs initialized in those configurations converge to the nonmagnetic ground state after geometry relaxation.

In the presence of the magnetic ordering at the edges, the nonmagnetic bands in ZGNRs are only slightly perturbed except the bands near E_F. Although the band structures of ZGNRs with even and odd number of layers look almost similar, they are different near E_F and the Brillouin zone edge. Nonmagnetic ZGNRs with an odd number of layers have nearly flat bands crossing E_F (Figure 4a,c). Such bands are not present in nonmagnetic ZGNRs with an even number of layers. This property is reminiscent of the different electronic structure of graphene multilayers, where Dirac fermions with a linear dispersion are present in graphene with an odd number of layers, while only normal fermions with a parabolic dispersion are present in graphene with an even number of layers.[23] Upon magnetic ordering at the ZGNR edges, the splitting of the bands crossing E_F is higher compared to that of the other flat bands slightly away from E_F. The band structures of ZGNRs with four or more layers are in close agreement with each other irrespective of their magnetic ordering (Figure 4d,h,l). This is also reflected in their total energies in Figure 3c, where the energy difference between nonmagnetic, AF−AF, and FM−AF orderings becomes very small as the number of layers increases beyond three.

The band gap of ZGNRs as a function of the number of layers is shown in Figure 5. As discussed earlier, only ZGNRs with AF−AF ordering and a nonmagnetic bilayer ZGNR have a band gap. Relaxed ZGNRs have a smaller band gap compared to unrelaxed ZGNRs. The GW-corrected band structures of a relaxed single-layer ZGNR with AF in-layer ordering and relaxed bilayer ZGNR, which has a nonmagnetic ground state, are shown in Figure 4e,f. The GW-corrected band gaps of single- and bilayer ZGNRs are also shown in Figure 5. The quasiparticle corrections for unrelaxed bilayer AF−AF ZGNRs are smaller compared to unrelaxed single-layer ZGNRs with AF in-layer ordering because each layer screens the Coulomb interactions in another layer, reducing the overall Coulomb effects.[36−40] Both the DFT and GW band gaps of a nonmagnetic relaxed bilayer ZGNRs are much smaller compared to unrelaxed bilayer ZGNR with AF−AF ordering.

Since the electronic structure of ZGNRs is mainly determined by the edge states,[16] ZGNRs with different widths are expected to show similar electronic structure evolution with the number of layers as ZGNR-8 discussed here. Ultranarrow ZGNRs may show different electronic structure evolution due to strong interedge interactions.

CONCLUSION

To summarize, the evolution of electronic properties of GNRs as a function of the number of layers stacked together is studied using DFT including van der Waals interactions. Multilayer AGNRs, similar to single-layer AGNRs, are found to exhibit three classes of band gaps depending on their width. In ZGNRs, the AF interlayer coupling is more stable compared to the FM interlayer coupling. ZGNRs with the FM in-layer and AF interlayer coupling do not have a band gap, while ZGNRs with the AF in-layer and AF interlayer coupling have a finite band gap, which decreases with increasing the number of layers. The magnetic stabilization energy decreases as the number of layers increases, indicating that the magnetic ordering is less stable in multilayer ZGNRs compared to single-layer ZGNRs. The ground state of the bilayer ZGNR is found to be nonmagnetic with a small but finite band gap. The DFT calculations, which do not include geometry relaxation, cannot predict the nonmagnetic ground state of a bilayer ZGNR and overestimate the band gap of multilayer ZGNRs in AF–AF configuration. The GW calculations on single- and bilayer GNRs indicate that the quasiparticle band gap corrections decrease with increasing number of layers due to the reduction in Coulomb effects.

METHODS

The electronic structure calculations are performed within the framework of first-principles density functional theory as implemented in the Vienna *ab initio* simulation package (VASP) code.[42,43] The PAW pseudopotentials[44,45] and the PBE exchange-correlation functional in the generalized gradient approximation[46] are used. The DFT-D2 method of Grimme[47] as implemented in VASP[48] is used to model the van der Waals interaction between GNR layers. To ensure negligible interaction between periodic images, a large value (10 Å) of the vacuum region is used. The 1D Brillouin zone of few-layer GNRs is sampled using 32 uniformly spaced *k*-points, while the 2D Brillouin zone of a multilayer GNR is sampled using $1 \times 16 \times 10$ Monkhorst-Pack mesh.[49] For the plane wave expansion of the wave function, a 400 eV kinetic energy cutoff is used. The total energy and the atomic force are converged to within 10^{-4} eV and 0.05 eV/Å, respectively. To obtain the band structure of few-layer GNRs, a non-self-consistent calculation is carried out on 101 uniformly spaced *k*-points in the positive half of the Brillouin zone using the converged charge density from the self-consistent calculation.

The GW calculations are performed using the ABINIT code.[50] The norm-conserving pseudopotentials generated using the Trouiller–Martins scheme[51] implemented in the fhi98PP pseudopotential program[52] are used. The PBE parametrization for the exchange-correlation functional[46] is used. To ensure negligible interaction between periodic images, a large value (10 Å) of the vacuum region is used. The Brillouin zone is sampled using 32 uniformly spaced *k*-points. For the plane wave expansion of the wave function, a 12 Ha kinetic energy cutoff is used. The DFT band structures calculated using VASP and ABINIT are virtually identical. The quasiparticle corrections are calculated within the G_0W_0 approximation, and the screening is calculated using the plasmon-pole model.[53] The Coulomb cutoff technique proposed by Beigi *et al.*[54] is used to minimize the spurious interactions with periodic replicas of the system.

Acknowledgment. This work is supported partly by the Interconnect Focus Center funded by the MARCO program of SRC and State of New York, NSF PetaApps grant number 0749140, and an anonymous gift from Rensselaer. S.K. acknowledges financial support provided by NSF ECCS 1102481. Computing resources of the Computational Center for Nanotechnology Innovations at Rensselaer partly funded by State of New York and of nanoHUB.org funded by the National Science Foundation have been used for this work.

REFERENCES AND NOTES

1. Geim, A. K.; Novoselov, K. S. The Rise of Graphene. *Nat. Mater.* **2007**, *6*, 183–191.
2. Novoselov, K.; Geim, A.; Morozov, S.; Jiang, D.; Zhang, Y.; Dubonos, S.; Grigorieva, I.; Firsov, A. Electric Field Effect in Atomically Thin Carbon Films. *Science* **2004**, *306*, 666–669.
3. Novoselov, K.; Geim, A.; Morozov, S.; Jiang, D.; Katsnelson, M.; Grigorieva, I.; Dubonos, S.; Firsov, A. Two-Dimensional Gas of Massless Dirac Fermions in Graphene. *Nature* **2005**, *438*, 197–200.
4. Nair, R. R.; Blake, P.; Grigorenko, A. N.; Novoselov, K. S.; Booth, T. J.; Stauber, T.; Peres, N. M. R.; Geim, A. K. Fine Structure Constant Defines Visual Transparency of Graphene. *Science* **2008**, *320*, 1308.
5. Schedin, F.; Geim, A. K.; Morozov, S. V.; Hill, E. W.; Blake, P.; Katsnelson, M. I.; Novoselov, K. S. Detection of Individual Gas Molecules Adsorbed on Graphene. *Nat. Mater.* **2007**, *6*, 652–655.
6. Schwierz, F. Graphene Transistors. *Nat. Nanotechnol.* **2010**, *5*, 487–496.
7. Balandin, A. A.; Ghosh, S.; Bao, W.; Calizo, I.; Teweldebrhan, D.; Miao, F.; Lau, C. N. Superior Thermal Conductivity of Single-Layer Graphene. *Nano Lett.* **2008**, *8*, 902–907.
8. Shao, Q.; Liu, G.; Teweldebrhan, D.; Balandin, A. A. High-Temperature Quenching of Electrical Resistance in Graphene Interconnects. *Appl. Phys. Lett.* **2008**, *92*, 202108.
9. Murali, R.; Yang, Y.; Brenner, K.; Beck, T.; Meindl, J. D. Breakdown Current Density of Graphene Nanoribbons. *Appl. Phys. Lett.* **2009**, *94*, 243114.
10. ITRS, *International Technology Roadmap for Semiconductors*, **2009**.
11. Hernandez-Nieves, A. D.; Partoens, B.; Peeters, F. M. Electronic and Magnetic Properties of Superlattices of Graphene/Graphane Nanoribbons with Different Edge Hydrogenation. *Phys. Rev. B* **2010**, *82*, 165412.
12. Elias, D. C.; Nair, R. R.; Mohiuddin, T. M. G.; Morozov, S. V.; Blake, P.; Halsall, M. P.; Ferrari, A. C.; Boukhvalov, D. W.; Katsnelson, M. I.; Geim, A. K.; *et al.* Control of Graphene's Properties by Reversible Hydrogenation: Evidence for Graphane. *Science* **2009**, *323*, 610–613.
13. Cheng, S. H.; Zou, K.; Okino, F.; Gutierrez, H. R.; Gupta, A.; Shen, N.; Eklund, P. C.; Sofo, J. O.; Zhu, J. Reversible Fluorination of Graphene: Evidence of a Two-Dimensional Wide Bandgap Semiconductor. *Phys. Rev. B* **2010**, *81*, 205435.
14. Robinson, J. T.; Burgess, J. S.; Junkermeier, C. E.; Badescu, S. C.; Reinecke, T. L.; Perkins, F. K.; Zalalutdniov, M. K.; Baldwin, J. W.; Culbertson, J. C.; Sheehan, P. E.; *et al.* Properties of Fluorinated Graphene Films. *Nano Lett.* **2010**, *10*, 3001–3005.
15. Han, M. Y.; Oezyilmaz, B.; Zhang, Y.; Kim, P. Energy Band-Gap Engineering of Graphene Nanoribbons. *Phys. Rev. Lett.* **2007**, *98*, 206805.
16. Son, Y.-W.; Cohen, M. L.; Louie, S. G. Energy Gaps in Graphene Nanoribbons. *Phys. Rev. Lett.* **2006**, *97*, 216803.
17. Yang, L.; Park, C.-H.; Son, Y.-W.; Cohen, M. L.; Louie, S. G. Quasiparticle Energies and Band Gaps in Graphene Nanoribbons. *Phys. Rev. Lett.* **2007**, *99*, 186801.
18. Son, Y.-W.; Cohen, M. L.; Louie, S. G. Half-Metallic Graphene Nanoribbons. *Nature* **2006**, *444*, 347–349.
19. Shimizu, T.; Haruyama, J.; Marcano, D. C.; Kosinkin, D. V.; Tour, J. M.; Hirose, K.; Suenaga, K. Large Intrinsic Energy Bandgaps in Annealed Nanotube-Derived Graphene Nanoribbons. *Nat. Nanotechnol.* **2011**, *6*, 45–50.
20. Tao, C.; Jiao, L.; Yazyev, O. V.; Chen, Y. C.; Feng, J.; Zhang, X.; Capaz, R. B.; Tour, J. M.; Zettl, A.; Louie, S. G.; *et al.* Spatially

Resolving Edge States of Chiral Graphene Nanoribbons. *Nat. Phys.* **2011**, doi 10.1038/nphys1991.
21. Partoens, B.; Peeters, F. M. From Graphene to Graphite: Electronic Structure Around the K Point. *Phys. Rev. B* **2006**, *74*, 075404.
22. Latil, S.; Henrard, L. Charge Carriers in Few-Layer Graphene Films. *Phys. Rev. Lett.* **2006**, *97*, 036803.
23. Partoens, B.; Peeters, F. M. Normal and Dirac Fermions in Graphene Multilayers: Tight-Binding Description of the Electronic Structure. *Phys. Rev. B* **2007**, *75*, 193402.
24. Grueneis, A.; Attaccalite, C.; Wirtz, L.; Shiozawa, H.; Saito, R.; Pichler, T.; Rubio, A. Tight-Binding Description of the Quasiparticle Dispersion of Graphite and Few-Layer Graphene. *Phys. Rev. B* **2008**, *78*, 205425.
25. Avetisyan, A. A.; Partoens, B.; Peeters, F. M. Stacking Order Dependent Electric Field Tuning of the Band Gap in Graphene Multilayers. *Phys. Rev. B* **2010**, *81*, 115432.
26. Zhang, Y.; Tang, T.-T.; Girit, C.; Hao, Z.; Martin, M. C.; Zettl, A.; Crommie, M. F.; Shen, Y. R.; Wang, F. Direct Observation of a Widely Tunable Bandgap in Bilayer Graphene. *Nature* **2009**, *459*, 820–823.
27. Craciun, M. F.; Russo, S.; Yamamoto, M.; Oostinga, J. B.; Morpurgo, A. F.; Thrucha, S. Trilayer Graphene is a Semimetal with a Gate-Tunable Band Overlap. *Nat. Nanotechnol.* **2009**, *4*, 383–388.
28. Mak, K. F.; Sfeir, M. Y.; Misewich, J. A.; Heinz, T. F. The Evolution of Electronic Structure in Few-Layer Graphene Revealed by Optical Spectroscopy. *Proc. Natl. Acad. Sci. U.S.A.* **2010**, *107*, 14999–15004.
29. Wang, H. M.; Wu, Y. H.; Ni, Z. H.; Shen, Z. X. Electronic Transport and Layer Engineering in Multilayer Graphene Structures. *Appl. Phys. Lett.* **2008**, *92*, 053504.
30. Lam, K.-T.; Liang, G. An Ab Initio Study on Energy Gap of Bilayer Graphene Nanoribbons with Armchair Edges. *Appl. Phys. Lett.* **2008**, *92*, 223106.
31. Lima, M. P.; Fazzio, A.; da Silva, A. J. R. Edge Effects in Bilayer Graphene Nanoribbons: *Ab Initio* Total-Energy Density Functional Theory Calculations. *Phys. Rev. B* **2009**, *79*, 153401.
32. Lee, H.; Son, Y.; Park, N.; Han, S.; Yu, J. Magnetic Ordering at the Edges of Graphitic Fragments: Magnetic Tail Interactions between the Edge-Localized States. *Phys. Rev. B* **2005**, *72*, 174431.
33. Sahu, B.; Min, H.; MacDonald, A. H.; Banerjee, S. K. Energy Gaps, Magnetism, and Electric-Field Effects in Bilayer Graphene Nanoribbons. *Phys. Rev. B* **2008**, *78*, 045404.
34. Zhang, Z.; Chen, C.; Zeng, X. C.; Guo, W. Tuning the Magnetic and Electronic Properties of Bilayer Graphene Nanoribbons on Si(001) by Bias Voltage. *Phys. Rev. B* **2010**, *81*, 155428.
35. Sahu, B.; Min, H.; Banerjee, S. K. Effects of Edge Magnetism and External Electric Field on Energy Gaps in Multilayer Graphene Nanoribbons. *Phys. Rev. B* **2010**, *82*, 115426.
36. Neaton, J. B.; Hybertsen, M. S.; Louie, S. G. Renormalization of Molecular Electronic Levels at Metal–Molecule Interfaces. *Phys. Rev. Lett.* **2006**, *97*, 216405.
37. Thygesen, K. S.; Rubio, A. Renormalization of Molecular Quasiparticle Levels at Metal–Molecule Interfaces: Trends across Binding Regimes. *Phys. Rev. Lett.* **2009**, *102*, 046802.
38. Garcia-Lastra, J. M.; Rostgaard, C.; Rubio, A.; Thygesen, K. S. Polarization-Induced Renormalization of Molecular Levels at Metallic and Semiconducting Surfaces. *Phys. Rev. B* **2009**, *80*, 245427.
39. Freysoldt, C.; Rinke, P.; Scheffler, M. Controlling Polarization at Insulating Surfaces: Quasiparticle Calculations for Molecules Adsorbed on Insulator Films. *Phys. Rev. Lett.* **2009**, *103*, 056803.
40. Li, Y.; Lu, D.; Galli, G. Calculation of Quasi-Particle Energies of Aromatic Self-Assembled Monolayers on Au(111). *J. Chem. Theory Comput.* **2009**, *5*, 881–886.
41. Lee, H.; Park, N.; Son, Y.; Han, S.; Yu, J. Ferromagnetism at the Edges of the Stacked Graphitic Fragments: An *Ab Initio* Study. *Chem. Phys. Lett.* **2004**, *398*, 207–211.
42. Kresse, G.; Furthmüller, J. Efficiency of *Ab-Initio* Total Energy Calculations for Metals and Semiconductors Using a Plane-Wave Basis Set. *Comput. Mater. Sci.* **1996**, *6*, 15–50.
43. Kresse, G.; Furthmüller, J. Efficient Iterative Schemes for *Ab Initio* Total-Energy Calculations Using a Plane-Wave Basis Set. *Phys. Rev. B* **1996**, *54*, 11169–11186.
44. Blochl, P. Projector Augmented-Wave Method. *Phys. Rev. B* **1994**, *50*, 17953–17979.
45. Kresse, G.; Joubert, D. From Ultrasoft Pseudopotentials to the Projector Augmented-Wave Method. *Phys. Rev. B* **1999**, *59*, 1758–1775.
46. Perdew, J.; Burke, K.; Ernzerhof, M. Generalized Gradient Approximation Made Simple. *Phys. Rev. Lett.* **1996**, *77*, 3865–3868.
47. Grimme, S. Semiempirical GGA-Type Density Functional Constructed with a Long-Range Dispersion Correction. *J. Comput. Chem.* **2006**, *27*, 1787–1799.
48. Bucko, T.; Hafner, J.; Lebegue, S.; Angyan, J. G. Improved Description of the Structure of Molecular and Layered Crystals: *Ab Initio* DFT Calculations with van der Waals Corrections. *J. Phys. Chem. A* **2010**, *114*, 11814–11824.
49. Monkhorst, H.; Pack, J. Special Points for Brillouin-Zone Integrations. *Phys. Rev. B* **1976**, *13*, 5188–5192.
50. Gonze, X.; Amadon, B.; Anglade, P. M.; Beuken, J. M.; Bottin, F.; Boulanger, P.; Bruneval, F.; Caliste, D.; Caracas, R.; Cote, M.; *et al.* ABINIT: First-Principles Approach to Material and Nanosystem Properties. *Comput. Phys. Commun.* **2009**, *180*, 2582–2615.
51. Troullier, N.; Martins, J. L. Efficient Pseudopotentials for Plane-Wave Calculations. *Phys. Rev. B* **1991**, *43*, 1993–2006.
52. Fuchs, M.; Scheffler, M. *Ab Initio* Pseudopotentials for Electronic Structure Calculations of Poly-Atomic Systems Using Density-Functional Theory. *Comput. Phys. Commun.* **1999**, *119*, 67–98.
53. Hybertsen, M. S.; Louie, S. Electron Correlation in Semiconductors and Insulators: Band Gaps and Quasiparticle Energies. *Phys. Rev. B* **1986**, *34*, 5390–5413.
54. Ismail-Beigi, S. Truncation of Periodic Image Interactions for Confined Systems. *Phys. Rev. B* **2006**, *73*, 233103.